Published in final edited form as:
Q J R Meteorol Soc. 2017 April ; 143(705): 1746–1755. doi:10.1002/qj.3027.

An Idealised Test Case For Assessing The Linearization of Tracer Transport Schemes in NWP Models

James Kent[a,*] and **Daniel Holdaway**[b,c]

[a]Computing and Mathematics, University of South Wales, Pontypridd, UK

[b]Global Modeling and Assimilation Office, NASA Goddard Space Flight Center, MD, USA

[c]Goddard Earth Sciences Technology and Research, Universities Space Research Association, MD, USA

Abstract

The linearized version of a Numerical Weather Prediction (NWP) model, which consists of its tangent linear model (TLM) and adjoint, has a number of important applications in atmospheric modelling. As such it is important that the linearized version of the NWP model can provide an accurate representation of the perturbation growth that occurs in the nonlinear model and does not introduce spurious instability. A suite of test cases, built upon existing frameworks, are developed to assess the accuracy of the linearization of the tracer transport component of the NWP model. Deformation velocities are prescribed that return the tracer back to the initial conditions, thus providing an analytical solution. A selection of smooth and discontinuous tracers and tracer perturbations are used.

Example results are shown using second-order and third-order tracer transport schemes, both with and without nonlinear flux limiters. Metrics are offered for assessing the skill of the linearization and predicting when problems will occur. For the example schemes used the results show that linearizations of the nonlinear flux-limited transport schemes behave poorly due to the presence of unstable modes. Some linearized model implementation strategies are offered for situations where the nonlinear scheme should not be linearized.

Keywords

NWP; dynamics; advection; adjoint; TLM; linearization

1. Introduction

Numerical weather prediction models consist of several important components. These include the dynamics, which represent the large scale resolved part of the flow; the physics, representing the unresolved sub-grid scale processes; and the data assimilation, the formation of the initial conditions from observations and previous forecasts. For practical reasons, efforts towards the development of these various components often proceeds with

*Correspondence to: School of Computing and Mathematics, University of South Wales, Pontypridd, CF37 1DL, UK, james.kent@southwales.ac.uk.

little interaction between them. This can lead to inconsistencies or even incompatibility. One such example of this being problematic is when techniques used in the modeling of the dynamics and physics are incompatible with the data assimilation system. Data assimilation systems, whether based on ensemble or variational methods, make certain assumptions. These include that the model behaves linearly between analysis times and that fields and errors have Gaussian probability densities (Lorenc 1986). Indeed the 4DVAR variational technique relies directly on the tangent linear model (TLM) and adjoint of the Numerical Weather Prediction (NWP) model. Beyond representing the inherent nonlinear behaviour of the atmosphere, models often rely on the use of highly nonlinear numerics. This can be to achieve the modeling of discrete-like behavior, as in the moist physics (Holdaway *et al.* 2015), or to control something undesirable, such as the removal of negative tracer densities. Note that there are ongoing attempts to overcome some of the assumptions fundamental in current data assimilation, though computational efficiency remains a significant challenge (Van Leeuwen 2009).

A key component of the dynamical core is the advection, or transport, scheme. This is a process that is linear under constant forcing. Errico *et al.* (1993) demonstrated very high correlations when comparing the TLM and nonlinear model for a dry dynamical core with advection. However, it is known that linear positive definite advection schemes cannot be greater than first order (Godunov 1959), or more specifically that higher order shape preserving schemes are always nonlinear (Thuburn and Haine 2001). In modern applications nonlinear limiters (see, for example, van Leer (1974, 1977); Boris and Book (1973); Colella and Woodward (1984)) are used to preserve sharp gradients and to ensure positivity and/or monotonicity. Tracer mixing ratios and tracer densities are always positive, therefore these nonlinear limiters are required for high-order tracer transport algorithms. The high degree of nonlinearity and linear instability present in these commonly used schemes has been demonstrated for a one-dimensional tracer (Holdaway and Kent 2015). Not only does the presence of nonlinearity in these schemes prevent linearized versions of the schemes being useful but also potentially presents an inconsistency with the data assimilation assumptions.

In this paper we provide an idealized framework in which to test transport schemes for dynamical cores, while also testing how well a linearization performs. This will provide insight into how particular schemes may compare in the context of a complete numerical weather prediction system, rather than the more isolated case studies presently done. The transport scheme has strong links to the chemistry model (Ovtchinnikov and Easter 2009), and the advection of trace gases, clouds and aerosols in the atmosphere is a necessary part of any climate model (Lamarque *et al.* 2008). Development of the data assimilation of trace gases, aerosols and clouds is under way at many operational centers so it is important to understand how nonlinearity in the transport scheme might impact this. In addition to testing the nonlinear transport schemes, the framework outlined here is designed to assist the development of the linearization of transport schemes. Many centers are interested in developing adjoints for 4DVAR, observation impacts and studies of sensitivity to initial conditions. Using the tests presented here the linearization of a transport scheme can be rigorously tested and a suitable linearization put in place.

Many idealized test cases have been developed to aid in the assessment of NWP model dynamical cores (Jablonowski and Williamson 2006; Lauritzen *et al*. 2010; Williamson *et al*. 1992) and of tracer transport schemes (Nair and Jablonowski 2008; Nair and Lauritzen 2010; Kent *et al*. 2012, 2014; Lauritzen *et al*. 2015). There are many metrics that can be used in these test cases, such as the preservation of nonlinearly correlated trace species (Lauritzen and Thuburn 2012) or the consistency of the tracer with the dynamic variables (Whitehead *et al*. 2015). Here we present an idealized test case framework that consists of two-dimensional horizontal transport on the sphere, following the setup of Nair and Lauritzen (2010). The tests first described by Nair and Lauritzen (2010) have become a standard in assessing tracer transport schemes (see Lauritzen *et al*. (2014)). By prescribing certain velocities it is possible to create analytical solutions for both the nonlinear and linearized versions of the model.

The performance of the linearization of a model is typically measured by comparing the evolution of the linear and nonlinear perturbation trajectories. The linear perturbation trajectory is obtained by integrating an initial perturbation with the TLM; the nonlinear perturbation trajectory is the difference between two nonlinear model integrations, separated by the perturbation at initial time. The validity of the adjoint is tested by a dot product comparison with the TLM. Here we can make additional use of knowledge of the analytical solution. This means both the linearized and nonlinear perturbation trajectories can be compared with the true perturbation trajectory. As such some general linearity characteristics of a given scheme can be analyzed without linearizing the scheme but by comparing the nonlinear perturbation trajectory with the true perturbation trajectory. The linearization of the scheme can be examined by comparing the linear perturbation trajectory with both nonlinear and truth perturbation trajectories. In realistic applications it is likely that some linear transport scheme will be chosen for the linearized version of the model. The framework presented here will allow for a comparison of different linear schemes against both the nonlinear counterpart and the truth. Perturbation structures are compared for the test cases using correlations and normalized errors. Linear stability of the tangent linear model is also examined through the use of Eigenvalues.

This paper is structured as follows. Section 2 describes the governing equations for tracer transport on the sphere. A full description of the test case, using the prescribed velocities of Nair and Lauritzen (2010), is given in Section 3. Example results for this test case are provided in Section 4, and using Eigenvalues to determine linear stability is shown in Section 5. Section 6 demonstrates how using separate schemes for the nonlinear trajectory and the TLM may improve results by applying the test case to the work of Holdaway and Kent (2015). Finally, conclusions are drawn in Section 7.

2. The Advection Equation and Schemes

Two-dimensional tracer transport is governed by the continuity equation and the tracer conservation equation. The continuity equation is given as

$$\frac{\partial \rho}{\partial t} + \nabla \cdot (\mathbf{v}\rho) = 0, \quad (1)$$

where ρ is the density, ∇ is the two-dimensional gradient operator, t is time, and $\mathbf{v}$ is the two-dimensional velocity vector. In the absence of sources and sinks, the tracer conservation equation is given as

$$\frac{\partial \rho q}{\partial t} + \nabla \cdot (\mathbf{v}\rho q) = 0, \quad (2)$$

where q is the tracer mixing ratio. The tracer advection equation can be derived from (1) and (2), and can be written in advective form as

$$\frac{\partial q}{\partial t} + \mathbf{v} \cdot \nabla q = 0. \quad (3)$$

In spherical coordinates, the tracer advection equation becomes

$$\frac{\partial q}{\partial t} + \frac{u}{a\cos\varphi}\frac{\partial q}{\partial \lambda} + \frac{v}{a}\frac{\partial q}{\partial \varphi} = 0 \quad (4)$$

where λ is longitude, ϕ is latitude, u is the zonal velocity, v is the meridional velocity, and a is the radius of the sphere (in this case, the Earth).

Model variables are linearized by splitting into a reference part (denoted with a superscript r) and a perturbation part (denoted with a prime). Once expanded, any terms that do not consist of exactly one perturbation quantity are neglected. See the appendix for a discussion of the linearization process. For this paper we only consider a reference velocity, i.e. $u = u^r$ and $v = v^r$. Note that the reference parts are not required to be constant. The tracer mixing ratio becomes $q = q^r + q'$. The linearized version of equation (4) is,

$$\frac{\partial q'}{\partial t} + \frac{u}{a\cos\varphi}\frac{\partial q'}{\partial \lambda} + \frac{v}{a}\frac{\partial q'}{\partial \varphi} = 0. \quad (5)$$

Following Holdaway and Kent (2015), the semi-discretised linearized advection equation (5) can be written in vector form

$$\frac{\partial \mathbf{q}'}{\partial t} = \mathbf{M}\mathbf{q}', \quad (6)$$

where $\mathbf{q}'$ is the vector containing q' at all discrete locations on the sphere. The matrix $\mathbf{M}$ is the operator of the tangent linear model, containing u^r and v^r as well as the horizontal derivative operators.

With constant velocities equation (3) and equation (4) are linear, but nonlinearity could be present in the numerical solution due to the use of a limiter. If a numerical scheme solves the general continuous nonlinear advection equation as

$$\frac{\partial \mathbf{q}}{\partial t} = \mathbf{m}(\mathbf{q}), \quad (7)$$

where $\mathbf{m}$ is the operator of the scheme, then a linear numerical scheme has the property

$$\mathbf{m}(\mathbf{q}') = \mathbf{M}\mathbf{q}'. \quad (8)$$

As the operator of the tangent linear model may depend on q^r, this can be rewritten as

$$\mathbf{m}(\mathbf{q}) - \mathbf{m}(\mathbf{q}^r) = \mathbf{M}\mathbf{q}'. \quad (9)$$

2.1. Numerical Schemes

We provide example results using four different numerical methods. We use different orders of accuracy (Holdaway *et al.* 2008) and both linear and nonlinear methods. For simplicity, all testing is performed on a latitude-longitude grid.

We use the Lax-Wendroff scheme (Lax and Wendroff 1960; Crowley 1968) in two-dimensional form (Smolarkiewicz 1982). This scheme is both linear and second-order accurate. To make this scheme nonlinear we can apply the multidimensional flux limiter of Thuburn (1996). The Appendix outlines the linearization of the Lax-Wendroff scheme with this limiter. We also make use of the linear third-order scheme UTOPIA (Leonard *et al.* 1993). Again, this can be made nonlinear by applying the flux limiter of Thuburn (1996). We refer to the nonlinear flux-limiter schemes as *limited*.

The tangent linear versions of these transport schemes can be obtained either manually in a line-by-line manner or by using the Tapenade auto differentiation tool (Hascoet and Pascual 2013). In both cases the exact tangent linear of the code will be obtained. Though the produced code is technically correct, when discontinuities exist the linearization will be inaccurate and could be unstable, as is the case for many limited advection schemes. The test cases below can be used to evaluate whether the linearization should be used and if not how an alternative approach will perform.

3. Test Case Specification

The aim of the testing is to assess the accuracy of the tangent linear model of a tracer transport scheme in NWP contexts. This can be achieved by building upon the method of

Holdaway and Kent (2015), and expanding to two-dimensional flow on the sphere. For this testing two model runs are required for the full tracer transport scheme; Equation (3) is solved once for the full tracer mixing ratio q, and once for the reference part q^r. Note that if the tracer conservation equation (2) is used, then the density is constant and set as $\rho = 1$ for all testing. The initial conditions specified here describe the tracer mixing ratio perturbation q' and reference part q^r, where $q = q^r + q'$. Once the simulations of q and q^r have taken place using the full numerical scheme, a numerical solution of the tracer perturbation can be calculated as

$$q_N - q_N^r = q'_N, \quad (10)$$

where the subscript N indicates a solution using the full (possibly nonlinear) numerical scheme. A third run takes place using the TLM of the numerical scheme for the perturbation, calculating q'_L, where subscript L indicates the TLM of the scheme. A linear numerical scheme will have the property that

$$q_N - q_N^r = q'_L. \quad (11)$$

For prescribed velocities u and v (note that as $u = u^r$ and $v = v^r$ we will drop the superscript r on the velocities) that reverse the flow over the course of the simulation, the analytical solution is just the initial conditions. Therefore we will have an analytical solution for the tracer, the reference tracer, and the tracer perturbation. These analytical solutions are denoted with a subscript T.

It is standard to compare the tracer solution calculated with the numerical scheme, q_N, with the true analytical solution q_T (for example Lauritzen *et al.* (2012, 2014)), to calculate the accuracy of the numerical scheme. That is not the aim here. Here we are interested in the accuracy of the TLM and the suitability of using the TLM with the full scheme. We use two comparisons to show this: 1) comparing $q_N - q_N^r$ with q'_L will show the linearity of the full numerical scheme and the correlation between the full scheme and the TLM, and 2) comparing q'_L with q'_T will show the accuracy of the TLM.

The normalized ℓ_2 and ℓ_∞ error norms, defined as

$$\ell_2(\phi) = \sqrt{\frac{I[(\phi - \phi_D)^2]}{I[\phi_D^2]}}, \quad \ell_\infty(\phi) = \frac{\max |\phi - \phi_D|}{\max |\phi_D|}, \quad (12)$$

for a solution ϕ and a desired solution ϕ_D, are used as metrics in each test. Here $I[\phi]$ indicates the integral of ϕ over the surface of the sphere. For comparison 1) we set $\phi = q_N - q_N^r$ and $\phi_D = q'_L$ and for 2) we set $\phi = q'_L$ and $\phi_D = q'_T$. For simplicity, throughout

this manuscript we will call comparison 1) the *linearity error* and comparison 2) the *TLM error*.

We also calculate the correlation between the full scheme and the TLM using, where the summation is over all grid points,

$$C = \frac{\sum (q'_N q'_L)}{\sum (q'^2_N) \sum (q'^2_L)}. \quad (13)$$

3.1. Prescribed Velocities

For each test the velocities used are those given by Nair and Lauritzen (2010). This produces a strongly deformational flow with a background uniform flow. These prescribed winds have become a standard in testing tracer transport schemes on the sphere (see Lauritzen *et al.* (2012, 2014) and references within).

The velocities are given as

$$u(\lambda, \varphi, t) = \frac{10a}{T} \sin^2(\lambda') \sin(2\varphi) \cos\left(\frac{\pi t}{T}\right) + \frac{2\pi a}{T} \cos(\varphi), \quad (14)$$

$$v(\lambda, \varphi, t) = \frac{10a}{T} \sin(2\lambda') \cos(2\varphi) \cos\left(\frac{\pi t}{T}\right) \quad (15)$$

where a is the radius of the Earth, T is the length of the simulation (12 days to be consistent with the Lauritzen *et al.* (2014) testing), and $\lambda' = \lambda - 2\pi t/T$ is the horizontally translated longitude.

3.2. Initial Tracers

For these tests we use two sets of reference tracer: Gaussian hills, and slotted cylinders. This is to make use of both smooth and discontinuous data. For both sets of initial conditions the centres of the tracer are given as $(\lambda_{c1}, \varphi_{c1}) = (5\pi/6, 0)$ and $(\lambda_{c2}, \varphi_{c2}) = (7\pi/6, 0)$.

$$q^r(\lambda, \varphi) = q_0 \exp\left(-R\left[(\widetilde{X} - X_{C1})^2 + (\widetilde{Y} - Y_{C1})^2 + (\widetilde{Z} - Z_{C1})^2\right]\right) \quad (16)$$

$$+ q_0 \exp\left(-R\left[(\widetilde{X} - X_{C2})^2 + (\widetilde{Y} - Y_{C2})^2 + (\widetilde{Z} - Z_{C2})^2\right]\right) \quad (17)$$

The Gaussian hills are initialised as those in Levy *et al.* (2007), given in Eqn. (17), where $R = 5$, $q_0 = 1$ and

$$(\widetilde{X}, \widetilde{Y}, \widetilde{Z}) = (\cos\varphi\cos\lambda, \cos\varphi\sin\lambda, \sin\varphi)\,. \quad (18)$$

The centres X_{Ci}, Y_{Ci} and Z_{Ci} are calculated by replacing λ and φ in (18) with (λ_{ci}, φ_{ci}) for i = 1, 2.

The initialisation of the slotted cylinders is given in Eqn. (19), where r_i is the non-dimensional great circle distance to the different tracer centres,

$$r_i = \arccos(\sin\phi_{ci}\sin\phi + \cos\phi_{ci}\cos\phi\cos(\lambda - \lambda_{ci}))\,. \quad (20)$$

The initial condition for the Gaussian reference solution is shown in Figure 1 (a) and the initial condition for the slotted cylinder reference solution is shown in Figure 1 (b). Example results from the third-order UTOPIA scheme, to demonstrate the numerical evolution of the slotted cylinder reference tracer, are shown in Figure 2.

3.3. Initial Perturbations

In total 4 separate sets of initial conditions are performed for the complete testing: the transport of both of the reference tracers (Gaussian hills and slotted cylinders) with two types of the perturbation (Gaussian and step). As stated above, for each simulation we must run the full transport scheme for q and q^r, and the TLM for q'. The total time of each run is T = 12 days.

The nonlinear limiters typically work by assessing the gradients of the underlying field. If the perturbation has the same structure as the underlying reference solution then the limiters will be correctly aligned to maintain the shape of the perturbation too, even if the magnitude is different. Unfortunately this is not very realistic. For example, in data assimilation applications the analysis increment will rarely have the same structure as the background. Performing the experiments described here for a perturbation that is simply a scaling of the reference solution will erroneously lead to concluding the TLM performs well. It is realistic to assume the perturbations will lie in the vicinity of existing structure so we overlay perturbations on the reference solution. This will also reveal how the limiters interact with the evolving perturbation. If the perturbation is located far away from the reference solution then its evolution may well be linear since the limiters wont be active there.

To make the Gaussian perturbations distinct from the reference field they are initialized using (17) but with $q_0 = 10^{-4}$ and R = 10. The step function perturbation is given by

$$q'(\lambda, \varphi) = \begin{cases} b_0 & \text{if } r_i \le 1/4, \text{ for i} = 1, 2 \\ 0 & \text{otherwise} \end{cases}, \quad (21)$$

with $b_0 = 10^{-4}$. The Gaussian initial perturbation is shown in Figure 1 (c) and the step initial perturbation is shown in Figure 1 (d).

3.4. Running The Tests

Below we list the steps required to complete the testing described in this paper.

1. Using the full transport scheme calculate q_N
2. Using the full transport scheme calculate q_N^r
3. Using the transport scheme TLM calculate q_L'
4. Calculate the linearity error and TLM error using equation (12)
5. Calculate the correlation using equation (13)

The tests here are designed for two-dimensional transport on the sphere. However, they could be extended into three dimensions using the prescribed velocities given in Kent *et al.* (2014).

4. Example Results

The four different initial conditions (Gaussian and slotted cylinder reference tracers with Gaussian and step function perturbations)

$$q^r(\lambda,\varphi)=\begin{cases}1 & \text{if } r_i \le 1/2 \text{ and } \left|\lambda-\lambda_{ci}\right| \ge 1/12, \text{ for i} = 1,2\\ 1 & \text{if } r_1 \le 1/2 \text{ and } \left|\lambda-\lambda_{c1}\right| < 1/12 \text{ and } \phi-\phi_{c1} < -5/24,\\ 1 & \text{if } r_2 \le 1/2 \text{ and } \left|\lambda-\lambda_{c1}\right| < 1/12 \text{ and } \phi-\phi_{c2} > 5/24,\\ 0.1 & \text{otherwise}\end{cases} \tag{19}$$

are performed on a latitude longitude grid of 180 × 90 grid points, corresponding to 2° × 2° resolution. The time step used is $T/1440 = 720$ seconds.

4.1. Gaussian Reference

Results from the four numerical schemes for the Gaussian reference tracer with both the Gaussian and step perturbation are shown in Tables 1 and 2. The Tables present the normalized ℓ_2 and ℓ_∞ linearity error norms comparing $q_N - q_N^r$ with q_L', the correlation between q_N' and q_L', and the normalized ℓ_2/ℓ_∞ TLM error norms comparing q_L' with q_T'. Table 1 shows the results using the Gaussian perturbation, whereas Table 2 shows the results for the discontinuous step perturbation. For a linear scheme the correlation with the TLM is exact and the linearity error norms should be zero. For the Lax-Wendroff and UTOPIA schemes, both of which are linear, these metrics are zero to machine precision. For the schemes with limiters the UTOPIA scheme has the smallest ℓ_2 linearity error norms for both perturbation structures. Using the step function perturbation increases the linearity error norms for both of the limited schemes significantly. Even though the limited schemes are nonlinear, the correlations for both the Gaussian and step perturbations are 1 for all the schemes tested. These results show that with a smooth reference field the nonlinearities in the limited schemes are small.

The normalized ℓ_2/ℓ_∞ TLM error norms (comparing q'_L with q'_T) provides a measure of the accuracy of the TLM. For both perturbation types with the Gaussian reference the UTOPIA scheme's TLM outperforms that of the Lax-Wendroff scheme. This is expected as UTOPIA has a higher order-of-accuracy than Lax-Wendroff.

4.2. Slotted Cylinder Reference

The results using the slotted cylinder reference tracers are shown in Tables 3 and 4. As with the Gaussian reference tracer, normalized ℓ_2 and ℓ_∞ linearity error norms comparing $q_N - q_N^r$ with q'_L for the linear schemes are zero to machine precision. As the slotted cylinder reference tracer is discontinuous, this leads to the constant activation of the flux limiter in the nonlinear schemes with limiters. However, the discontinuities of the reference tracer do not align with any discontinuities of the perturbations, and therefore the ℓ_2 linearity error norms for the schemes with limiters are significantly larger than for the Gaussian hills reference tracer. The UTOPIA limiter scheme has worse correlations than the Lax-Wendroff limiter scheme. Figure 3 shows both $q_N - q_N^r$ and q'_L for the step perturbation simulated using the UTOPIA limiter scheme, with the left hand plots showing the results for the 720 s time step that is used to populate Tables 1–4. As the UTOPIA limiter scheme is nonlinear, the tangent linear perturbation q'_L, plot (c), has significant differences to the nonlinear perturbation trajectory, plot (a).

Comparing q'_L with q'_T, the TLM error, for the slotted cylinder reference tracers shows that the TLM for the UTOPIA limiter scheme outperforms the TLM of the Lax-Wendroff limiter scheme for all metrics apart from the ℓ_∞ norm for the step perturbation. This is generally consistent with the results for the Gaussian reference tracer. Note that the TLM error for the linear schemes does not depend on the reference tracer, hence the identical results for Lax-Wendroff and UTOPIA shown in Tables 2 and 4. The results from the testing with the slotted cylinder reference tracer show the poor performance of the nonlinear limited schemes.

The tests were repeated using larger perturbations, specifically $a_0 = b_0 = 0.2$ in equations (17) and (21). In general the results are similar to those presented for the smaller perturbations.

4.3. Resolution Sensitivity

To show the effect of model resolution on the TLM, we repeat the simulations for both the Gaussian hill reference tracer and slotted cylinder reference tracer, with the Gaussian perturbation. We use a grid of 360 × 180 grid points, corresponding to 1° × 1° resolution. The time step for this resolution is $T/2880 = 360$ seconds.

For both Lax-Wendroff and UTOPIA the normalised ℓ_2 linearity error norms are zero to machine precision, and the correlations are 1, for each test. The results for the limited schemes are presented in Table 5. For the Gaussian reference tracer the increase in resolution produces poorer ℓ_2 linearity errors and correlation statistics for the Lax-Wendroff limiter scheme. The UTOPIA limiter scheme shows no decrease in performance for the increased

resolution for the Gaussian reference tracer. For the slotted cylinder reference tracer with the Gaussian perturbation both the limited schemes produce much larger linearity error norms and poorer correlation statistics. The linearity error norms for both limited schemes are close to one, with corresponding correlations close to zero. These linearity error norms and correlations are significantly worse than those presented in Table 1 for the 2° × 2° grid resolution. This highlights how, for the non-smooth reference tracer, the nonlinearity of the limited schemes can increase with increased resolution. This could be problematic for data assimilation systems that try to use observations of clouds in very high resolution convection resolving models.

The accuracy of the TLM of the linear Lax-Wendroff and UTOPIA schemes improves with increased resolution, and so the normalised ℓ_2 TLM error norms for the linear schemes decrease. However, the accuracy of the TLM of the limited schemes decreases as the resolution increases. The ℓ_2 TLM error norms for the slotted cylinder reference tracer with the Gaussian perturbation are shown in Table 6 for the 2° × 2° and 1° × 1° resolution grids (corresponding to 180 × 90 and 360 × 180 grid points respectively). For the nonlinear schemes the TLM error norms increase dramatically with increased resolution. This highlights that the poor correlations shown in Table 5 for the limited schemes is due to the poor performance of the nonlinear schemes' TLMs.

Another consideration is that of temporal resolution. Figure 3 compares (top) $q_N - q_N^r$ with (bottom) q'_L for the UTOPIA limiter scheme for the slotted cylinder reference and step perturbation tracers on the 2° × 2° grid. The left hand plots are with a time step of $\Delta t = 720$ s, and the right hand plots are with $\Delta t = 360$ s. The top plots show that a change of time step has little effect on the nonlinear perturbation trajectory, $q_N - q_N^r$, for the limited UTOPIA scheme. However, the tangent linear perturbation q'_L develops significant errors due to the change in time step.

5. Eigenvalue Calculation and Growing Modes

In the previous section it is demonstrated that increasing resolution can result in a less accurate TLM. This is due in part to the presence of linear instability resulting from growing modes. Certain advection schemes support these growing modes, causing the solution of the linearized equations to be unstable. Note that this would not always be revealed by comparing $q_N - q_N^r$ and q'_T. The number of solutions to the linearized equations depends on resolution. As resolution increases the number of growing modes increases and so the instability can occur more rapidly.

Seeking solutions of the form $q' \sim \exp(\lambda t)$ in Equation (6) gives,

$$\lambda \mathbf{q}' = \mathbf{M}\mathbf{q}' . \quad (22)$$

The eigenvalues of **M** give λ and the eigenvectors give solutions q'. The temporal change λ can be a complex quantity; the imaginary part gives the frequency of the solution and the

real part the amplitude. If $\Re(\lambda) > 0$ then that particular solution, or mode, is said to be linearly unstable. When unstable modes are present the perturbation can grow in amplitude. These growing modes also explain how a decrease in time step, and hence an increase in the number of steps, can lead to instability, as shown in panel (d) of Figure 3.

Eigenspectra were computed in Holdaway and Kent (2015) to demonstrate the issues encountered with the nonlinear piecewise parabolic method schemes (PPM, see Colella and Woodward (1984)). The same method can be performed here. However, for a 1 degree resolution grid there are 16,200 solutions and $\mathbf{M}$ contains 2.6244×10^8 variables. Computing eigenvalues of a matrix of this magnitude is not practical. Given that the above results demonstrate a decrease in TLM accuracy as resolution increases it is still informative to compute eigenvalues for a lower resolution case.

For the example presented here eigenvalues are computed for a 15° × 15° resolution grid (i.e. 24 × 12 grid points), and for a simplified solid body rotation test case. This domain size makes the calculation viable and a demonstration of growing modes is indicative of an issue at any resolution.

The solid body rotation test makes use of velocities from Williamson *et al.* (1992)

$$u(\lambda, \varphi, t) = \frac{2\pi a}{T}(\cos(\varphi)\cos(\alpha) + \sin(\varphi)\cos(\lambda)\sin(\alpha)), \quad (23)$$

$$u(\lambda, \varphi, t) = -\frac{2\pi a}{T}\sin(\lambda)\sin(\alpha), \quad (24)$$

where α is the angle of rotation. As with the tests in the previous Section the density is constant $\rho = 1$. The tracers used for this test are the Gaussian reference and Gaussian perturbation, and they can be initialised using equation (16). For both the reference and perturbation, only one Gaussian hill is used, and this is initialised at the point $(3\pi/2, 0)$. A second run using one slotted cylinder reference and one step perturbation, again initialised at $(3\pi/2, 0)$, is also used. A time series of the maximum real part of the eigenvalue will show any linear instability in the scheme.

The eigenvalue spectrum for the Gaussian reference solution and Gaussian perturbation on the 15° grid with $\alpha = 0$ are shown in Figure 4 (a) for the Lax-Wendroff and Lax-Wendroff limiter schemes. Figure 4 (b) shows more detail in the region where unstable modes ($\Re(\lambda) > 0$) occur. Both plots are sampled at time step 627, although results from other time steps are qualitatively similar. As can be seen in Figure 4 (b) the Lax-Wendroff limiter scheme supports solutions that are linearly unstable due to the eigenvalue with $\Re(\lambda) > 0$. Note that the Lax-Wendroff scheme without the limiter is a linear scheme, and so $\Re(\lambda) \leq 0$ for all λ. The time series of the maximum real part of the eigenvalue for the Lax-Wendroff limiter scheme, Figure 4 (c), shows the presence of growing modes throughout the integration. This is also the case for the UTOPIA limiter scheme (not shown). For the linear

Lax-Wendroff and UTOPIA schemes, the maximum real part of the eigenvalue never exceeds zero. Figure 5 shows the eigenvalue spectrum when using the slotted cylinder reference and step perturbation test case. It is clear that the frequency of growing modes is similar to the Gaussian tracers.

6. Strategy for Operational Models

An alternative approach is to use different schemes for the full transport and the TLM. This method was developed by Holdaway and Kent (2015) for use in the GEOS-5 linear model. A nonlinear scheme is used for the full tracer transport, and a separate linear scheme is used to create the TLM. In this section we test this method using the Lax-Wendroff and UTOPIA schemes and the tests developed in Section 3.

The first scheme will use Lax-Wendroff limiter for the full transport, and Lax-Wendroff (without limiter) for the TLM. The second scheme will use UTOPIA limiter for the full transport and UTOPIA (again, without limiter) for the TLM. These schemes are denoted *mixed* schemes. In both cases the same order-of-accuracy is used for the full transport and the TLM, similar to Holdaway and Kent (2015). We test these schemes using the slotted cylinder reference tracer with the Gaussian perturbation, at 2° × 2° and 1° × 1° resolutions.

Tables 7 and 8 show the ℓ_2 linearity errors, the correlation, and the ℓ_2 TLM errors for the mixed schemes for the slotted cylinder reference tracer with the Gaussian perturbation for the 180 × 90 and 360 × 180 resolution grids. These can be compared with Tables 3, 4 and 6, to show the performance of the mixed schemes against the limited schemes.

For the 180 × 90 grid, the Lax-Wendroff mixed scheme performs worse than Lax-Wendroff limiter scheme. This may be due to the large TLM error for the linear Lax-Wendroff scheme. At this resolution the UTOPIA mixed scheme has lower error norms and a higher correlation than the UTOPIA limiter scheme. Increasing the resolution to 360 × 180 grid points shows the benefit of the mixed scheme. Even though the Lax-Wendroff mixed scheme has large error norms they are much lower than the Lax-Wendroff limiter scheme. The UTOPIA mixed scheme significantly outperforms the UTOPIA limiter scheme. The ℓ_2 TLM error for the mixed schemes is identical to the linear schemes (as the mixed scheme make use of the linear scheme's TLM), hence the good performance of the UTOPIA mix scheme.

Using a linear scheme to evolve the perturbations and a nonlinear scheme to evolve the trajectory avoids introducing instability. Importantly it also avoids introducing negative values and spurious oscillations into the trajectory, which would likely occur if using a linear scheme for both. The development of negative perturbation values is not an issue; indeed the initial conditions for the perturbation could be negative. However, the development of spurious oscillations in the perturbations is undesirable. In operational systems this could be ameliorated by applying explicit diffusion, for example stronger horizontal divergence damping, to the perturbation fields.

7. Discussion and Conclusions

A set of idealised tests have been developed to assess the accuracy of tracer transport schemes and their linearization. This is done by comparison of specific quantities: the nonlinear perturbation growth, tangent linear model (TLM) perturbation growth and the analytical perturbation growth. The tests put forward are based around an existing standard test case for tracer transport on the sphere (Nair and Lauritzen 2010), using the same prescribed velocities and reference tracers. A two dimensional setting captures the inherent issues associated with linearizing limited advection schemes, mimics how advection is performed in certain dynamical cores and facilitates an eigendecomposition of the operator. In addition to the normal integration of the transport scheme, two extra experiments are required in order to complete the testing. Firstly an additional integration of the nonlinear model is performed but where a perturbation is added to the initial conditions. Secondly an integration of the tangent linear model initialised with that same perturbation. The three measures are compared using error norms and correlations. Error norms are used to determine the ability of the full transport schemes to preserve the true perturbation structures as well as to estimate the linearity of the scheme by comparing with the truth. Correlations provide a bounded measure of how similar the nonlinear perturbation growth is to the TLM perturbation growth.

Example results are shown using second- and third-order transport schemes on the sphere. Each scheme is run with and without a flux limiter. The results show that the linear schemes have exact (to machine precision) correlation with their TLMs. For the schemes with limiters the error norms examining the correlation with the TLMs are large. The TLMs of the second-order schemes have larger error norms than those of the third-order schemes. Using discontinuous data, for example the slotted cylinders or step function, produces the largest error norms and the lowest correlations for the limited schemes. This is because the flux limiters are more active for the discontinuous data, resulting in a higher degree of nonlinearity. Interestingly it is noted that the accuracy of the TLM reduces as the resolution increases when the scheme in use is nonlinear. This is in contrast to tracer transport in general, where increases in resolution usually result in improved accuracy (see, for example Lauritzen *et al*. (2014)). An alternative approach, following Holdaway and Kent (2015), is to use a nonlinear scheme for the full transport and a linear scheme for the TLM. Using this approach with the third-order schemes produces lower error norms than just using the limited scheme, with a significant improvement for increased resolution.

Eigenvalue analysis is a useful tool that gives the set of solutions of a linearized set of equations. It reveals the spatial and temporal structures of the solutions and thus demonstrates whether unstable solutions exist. As well as providing insight into the behaviour of the model in general, it shows when a linearized version of a scheme may not be suitable. To facilitate computational efficiency the eigenvalue decomposition is performed for a 15° grid and using solid body rotation. For both limited schemes examined in this paper it is shown that a large number of growing modes are present. This explains why the perturbation grows in amplitude with these schemes and why problems can worsen with increased resolution.

These test cases put forward in this paper provide a framework for testing the nonlinearity of advection schemes. This can give insight into how particular schemes may perform when partnered with high resolution data assimilation and provides a testing environment for linearization strategies. The tests can show why numerical schemes that excel at tracer transport may not be suitable for use in a TLM.

Acknowledgments

We would like to thank Lucas Harris and one anonymous reviewer for their detailed comments that helped improve the manuscript.

Appendix

This appendix summarises the derivation of the tangent linear version of the second order Lax-Wendroff scheme with the limiter of Thuburn (1996). For simplicity the derivation is limited to the fluxes in the x-direction. The derivation is similar for the full two-or three-dimensional versions of the scheme.

The constant velocity, one dimensional second order Lax-Wendroff scheme in flux form is discretised as,

$$q_j^{n+1} = q_j^n - \frac{u\Delta t}{\Delta x}\left(F_{j+\frac{1}{2}} - F_{j-\frac{1}{2}}\right) \quad (25)$$

where the fluxes F are given by

$$F_{j+\frac{1}{2}} = \frac{1}{2}\left(q_{j+1}^n + q_j^n\right) - \frac{u\Delta t}{2\Delta x}\left(q_{j+1}^n + q_j^n\right). \quad (26)$$

Here j and n are the spatial and temporal indices respectively, Δx is the spatial grid spacing, and Δt is the time step. Equations (25) and (26) can be written in functional form as $q_j^{n+1} = m\left(q_1^n, q_2^n, \ldots, q_N^n\right)$, where the model m contains the outlined calculations. The change to the output when the input is perturbed is $\left(q_j^{n+1}\right)' = m[q_1^n + (q_1^n)', \ldots, q_N^n + (q_N^n)'] - m[q_1^n, \ldots, q_N^n]$. The $m[q_1^n + (q_1^n)', \ldots, q_N^n + (q_N^n)']$ term can be estimated using the first order Taylor series, reducing the calculation to $\left(q_j^{n+1}\right)' \approx \partial m/\partial q\big|_1^n (q_1^n)' + \ldots + \partial m/\partial q\big|_N^n (q_N^n)'$. This is the linearized form of the equations. Repeating for all j results in the matrix form $\mathbf{q}(n+1)' = \mathbf{M} \times (\mathbf{q}^n)'$, where $\mathbf{q}'$ contains q' at all points on the sphere and $\mathbf{M}$ contains all the derivatives.

To linearize the model the variables are expanded into the reference and perturbation parts, e.g. $q = q^r + q'$ and then all terms containing only reference variables or multiple perturbation terms are neglected. This is equivalent to computing the first order derivatives of m with respect to the model variables. Equation (25) when linearized is

$$\left(q_j^{n+1}\right)' = \left(q_j^n\right)' - \frac{u\Delta t}{\Delta x}\left(F'_{j+\frac{1}{2}} - F'_{j-\frac{1}{2}}\right). \quad (27)$$

The flux F is a function of q so must also be linearized,

$$F'_{j+2} = \frac{1}{2}\left[\left(q_{j+1}^n\right)' + \left(q_j^n\right)'\right] - \frac{u\Delta t}{2\Delta x}\left[\left(q_{j+1}^n\right)' - \left(q_j^n\right)'\right]. \quad (28)$$

It is clear that this second order unlimited part of the scheme is linear. The reference values q^r do not appear in the linearized equations and q' and q could be interchanged between the original and linearized equations, represented mathematically as $\mathbf{Mq}' \equiv \mathbf{m(q}')$. If the velocity u was not a fixed quantity but had a perturbation part u' then the system would be nonlinear. The linearized version of equation (25) would contain additional terms of the form $u'F\Delta t/\Delta x$. Even with u' terms the equations would only be considered weakly nonlinear since the linearization would remain accurate in the limit of small perturbations, $u', q' \ll 1$.

In the above form the scheme is non-monotonic and can develop negative values in the presence of steep gradients. A limiter is applied to the fluxes to give the scheme better shape preserving properties. The limiter used in this article is outlined by Thuburn (1996) for one-dimensional flow. As seen in equation (18) of Thuburn (1996), and using the same notation, the process begins by computing the minimum inflow bounds for the face L,

$$\left(q_L^{(\mathrm{in})}\right)'_{\min} = \begin{cases} q_i^n & \text{if } q_j^n \le q_{j+1}^n, \\ q_{i+1}^n & \text{if } q_{j+1}^n > q_j^n \end{cases}. \quad (29)$$

This piecewise linear equation is linearized as,

$$\left(q_L^{(\mathrm{in})}\right)'_{\min} = \begin{cases} \left(q_j^n\right)' & \text{if } \left(q_j^n\right)^r \le \left(q_{j+1}^n\right)^r, \\ \left(q_{j+1}^n\right)' & \text{if } \left(q_{j+1}^n\right)^r > \left(q_j^n\right)^r \end{cases}. \quad (30)$$

Note that now the linearized equations depend on reference values and there is clear nonlinearity through the use of a discrete switch. This is potentially a very strong nonlinearity in that the linearized model is not necessarily accurate in the limit of small perturbations. Indeed in the nonlinear model finite changes in $\left(q_L^{(\mathrm{in})}\right)'_{\min}$ are possible even when only infinitesimal changes are made to $\left(q_j^n\right)'$.

Ultimately the perturbation flux F' is modified and depends on $\left(q_L^{(\text{in})}\right)'_{\min}$ as well as other quantities depending on q' in a piecewise manner. This can be seen in equations (18) – (31) in Thuburn (1996). This limiter, as well as other kinds of limiters, apply these piecewise linear forms throughout and are considered highly nonlinear. Although the first order Taylor approximation is accurate away from the discontinuity it can not represent the affect of a perturbation that traverses the discontinuity, where it can become very inaccurate.

References

Boris JP, Book DL. Flux-corrected transport I. SHASTA, a fluid algorithm that works. J Comput Phys. 1973; 11:38–69.

Colella P, Woodward PR. The Piecewise Parabolic Method (PPM) for gas-dynamical simulations. J Comput Phys. 1984; 54:174–201.

Crowley WP. Numerical advection experiments. Mon Wea Rev. 1968; 96:1–11.

Errico R, Vukicevic T, Raeder K. Examination of the accuracy of a tangent linear model. Tellus A. 1993; 45A:462–477.

Godunov SK. Finite difference method for numerical computation of discontinuous solutions of the equations of fluid dynamics (in Russian). Math Sbornik. 1959; 47:271–360.

Hascoet L, Pascual V. The Tapenade automatic differentiation tool: principles, model, and specification. ACM Trans Math Softw. 2013; 39(20):1–20. 43.

Holdaway D, Errico R, Gelaro R, Kim JG, Mahajan R. A linearized prognostic cloud scheme in nasa's goddard earth observing system data assimilation tools. Mon Wea Rev. 2015; 142:414–433.

Holdaway D, Kent J. Assessing the tangent linear behavior of common tracer transport schemes and their use in a linearized atmospheric general circulation model. Tellus A. 2015; 67 27 895.

Holdaway D, Thuburn J, Wood N. On the relation between order of accuracy, convergence rate and spectral slope for linear numerical methods applied to multiscale problems. Int J Num Meth Fl. 2008; 56:1297–1303.

Jablonowski C, Williamson DL. A baroclinic instability test case for atmospheric model dynamical cores. Quart J Roy Meteor Soc. 2006; 132:2943–2975.

Kent J, Jablonowski C, Whitehead JP, Rood RB. Downscale cascades in tracer transport test cases: an intercomparison of the dynamical cores in the Community Atmosphere Model CAM5. Geo Model Dev. 2012; 5:1517–1530.

Kent J, Ullrich PA, Jablonowski C. Dynamical core model intercomparison project: Tracer transport test cases. Quart J Roy Meteor Soc. 2014; 140:1279–1293.

Lamarque JF, Kinnison DE, Hess PG, Vitt FM. Simulated lower stratospheric trends between 1970 and 2005: Identifying the role of climate and composition changes. J Geo Res. 2008; 113:D12 301.

Lauritzen PH, Conley AJ, Lamarque JF, Vitt F, Taylor MA. The terminator "toy"-chemistry test: A simple tool to assess errors in transport schemes. Geosci Model Dev. 2015; 8:1299–1313.

Lauritzen PH, Jablonowski CJ, Taylor MA, Nair RD. Rotated versions of the jablonowski steady-state and baroclinic wave test cases: A dynamical core intercomparison. J Adv Model Earth Syst. 2010; 2:34.

Lauritzen PH, Skamarock WC, Prather MJ, Taylor MA. A standard test case suite for two-dimensional linear transport on the sphere. Geosci Model Dev. 2012; 5:105–145.

Lauritzen PH, Thuburn J. Evaluating advection/transport schemes using interrelated tracers, scatter plots and numerical mixing diagnostics. Quart J Roy Meteor Soc. 2012; 138:906–918.

Lauritzen PH, Ullrich PA, Jablonowski C, Bosler PA, Calhoun D, Conley AJ, Enomoto T, Dong L, Dubey S, Guba O, Hansen AB, Kaas E, Kent J, Lamarque JF, Prather MJ, Reinert D, Shashkin VV, Skamarock WC, Sorensen B, Taylor MA, Tolstykh MA. A standard test case suite for two-dimensional linear transport on the sphere: Results from a collection of state-of-the-art schemes. Geosci Model Dev. 2014; 5:105–145.

Lax PD, Wendroff B. Systems of conservation laws. Commun Pure Appl Math. 1960; 13:217–237.

Leonard BP, MacVean MK, Lock AP. Positivity-preserving numerical schemes for multidimensional advection. Technical report, NASA Technical Memorandum 106055. 1993

Levy MN, Nair RD, Tufo HM. High-order galerkin method for scalable global atmospheric models. Comput Geosci. 2007; 33:1022–1035.

Lorenc AC. Analysis methods for numerical weather prediction. Quart J Roy Meteorol Soc. 1986; 112:1177–1194.

Nair RD, Jablonowski C. Moving vortices on the sphere: a test case for horizontal advection problems. Mon Wea Rev. 2008; 136:699–711.

Nair RD, Lauritzen PH. A class of deformational flow test cases for linear transport problems on the sphere. J Comput Phys. 2010; 229:8868–8887.

Ovtchinnikov M, Easter RC. Nonlinear advection algorithms applied to interrelated tracers: Errors and implications for modeling aerosol-cloud interactions. Mon Wea Rev. 2009; 137:632–644.

Smolarkiewicz PK. The multidimensional Crowley advection scheme. Mon Wea Rev. 1982; 110:1968–1983.

Thuburn J. Multidimensional flux-limited advection schemes. J Comput Phys. 1996; 23:74–83.

Thuburn J, Haine TWN. Adjoints of nonoscillatory advection schemes. J Comput Phys. 2001; 171:616–631.

van Leer B. Towards the ultimate conservative difference scheme. II. monotonicity and conservation combined in a second-order scheme. J Comput Phys. 1974; 14:361–370.

van Leer B. Towards the ultimate conservative difference scheme. III. upstream-centered finite-difference schemes for ideal compressible flow. J Comput Phys. 1977; 23:263–275.

Van Leeuwen P. Particle filtering in geophysical systems. Mon Wea Rev. 2009; 137:4089–4114.

Whitehead JP, Jablonowski C, Kent J, Rood RB. Potential vorticity: Measuring consistency between gcm dynamical cores and tracer advection schemes. Quart J Roy Meteor Soc. 2015; 141:739–751.

Williamson DL, Drake JB, Hack JJ, Jakob R, Swarztrauber PN. A standard test set for numerical approximations to the shallow water equations in spherical geometry. J Comput Phys. 1992; 102:211–224.

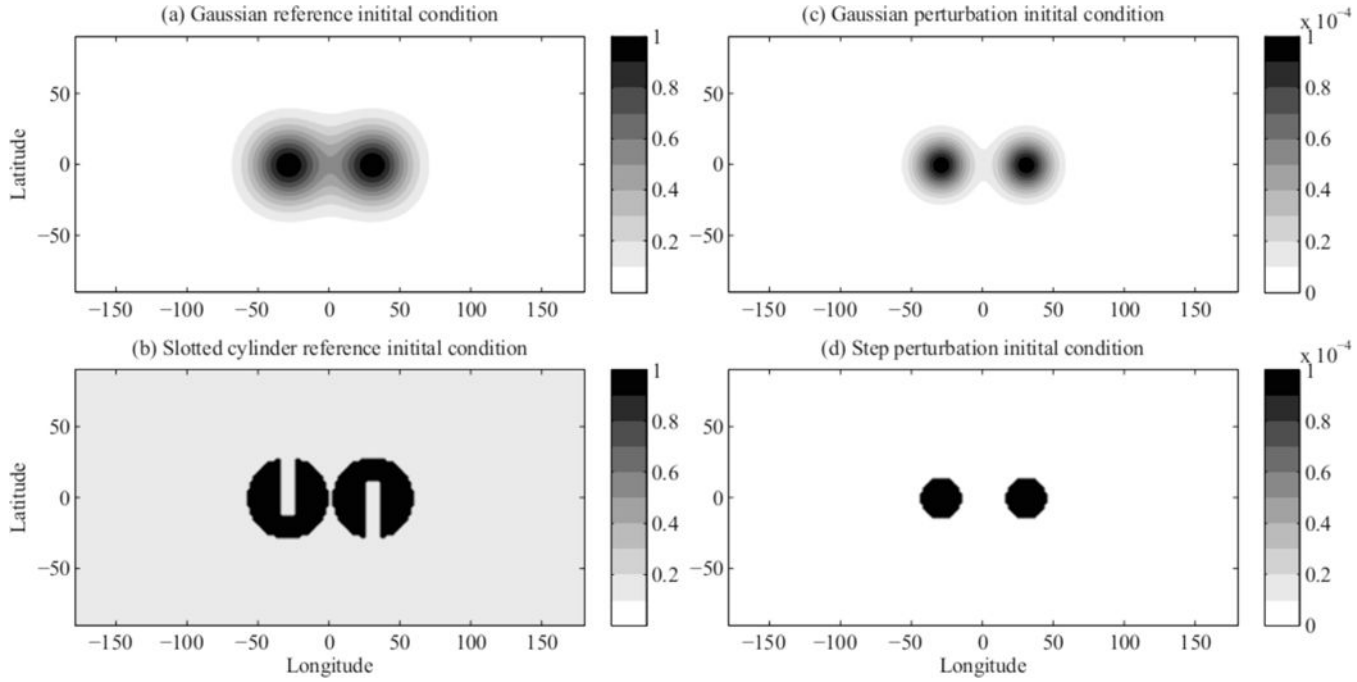

Figure 1.

(a) The Gaussian hill initial conditions for the reference part of the solution. (b) The slotted cylinder initial conditions for the reference solution. (c) The Gaussian hill initial conditions for the perturbation part of the solution. (d) The step perturbation initial conditions.

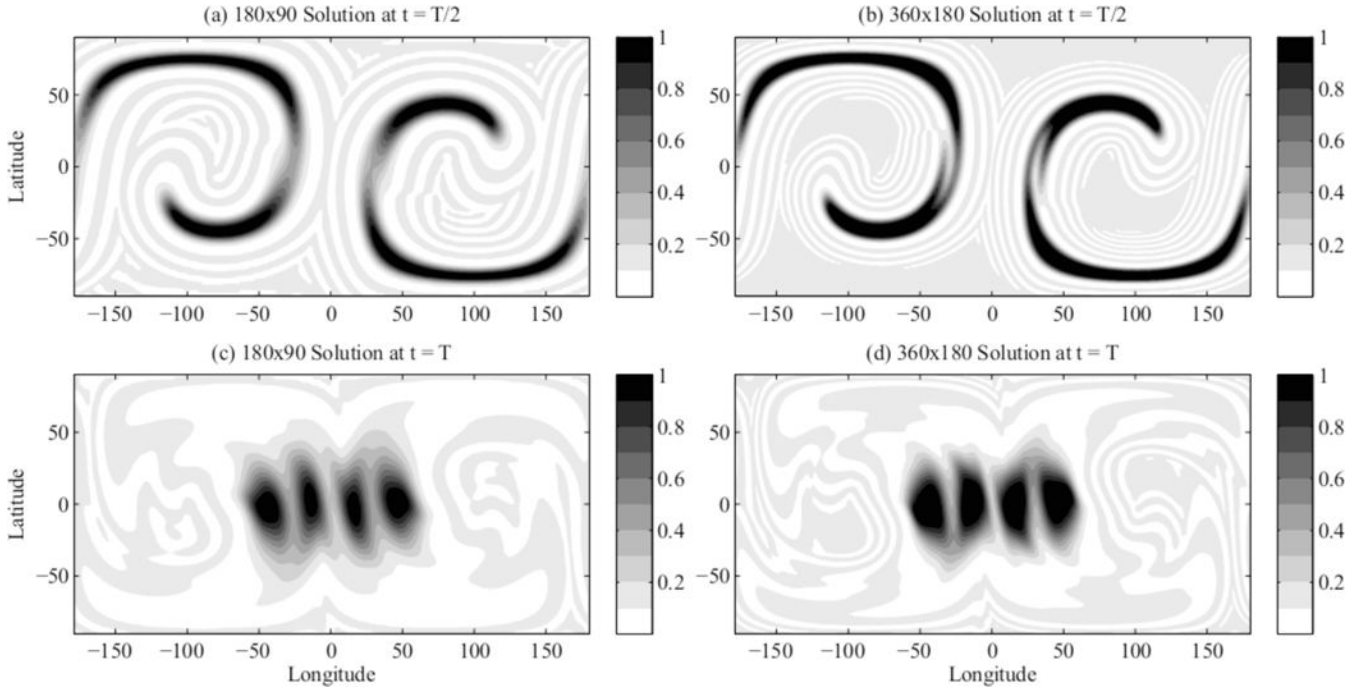

Figure 2.

The evolution of the slotted cylinder reference solution throughout the integration for the UTOPIA scheme on the 180 × 90 grid (a and c) and the 360 × 180 grid (b and c). Panels (a) and (b) show the solutions halfway through the integration and panels (c) and (d) show the end of the integration.

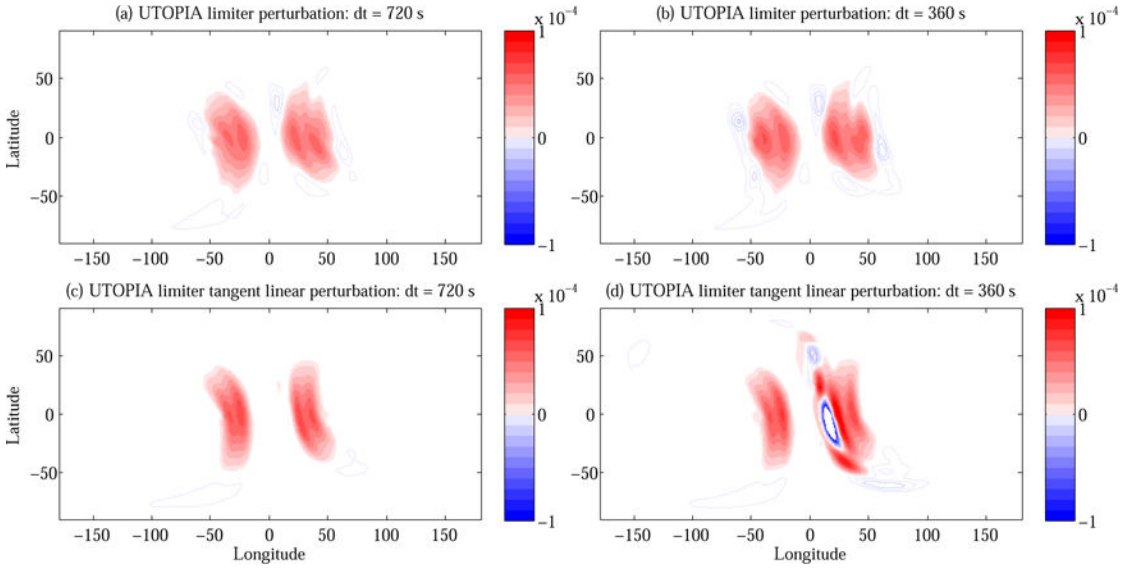

Figure 3.

Comparison of the (top) nonlinear perturbation trajectory $q_N - q_N^r$ and (bottom) tangent linear perturbation trajectory q_L' for the UTOPIA limiter scheme with the slotted cylinder reference solution and step perturbation on the 180 × 90 grid. The time steps used were (left) 720 s and (right) 360 s. The analytical solution for each plot is that of Figure 1 (d). Positive values of the perturbation are shaded and negative values are contoured.

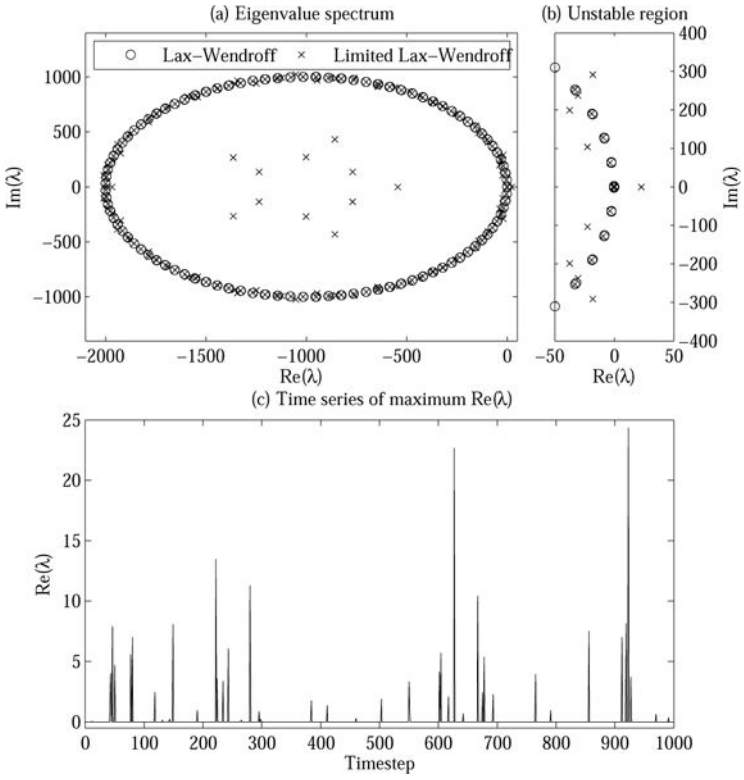

Figure 4.

(a) The eigenvalue spectrum for the Lax-Wendroff and limited Lax-Wendroff schemes at time step 627 for the Gaussian reference and perturbation tracers on the 20 × 10 grid. (b) as in (a) but showing the detail of the region related to instability. (c) Time series of the maximum real part of the eigenvalue at all time steps for the limited Lax-Wendroff scheme.

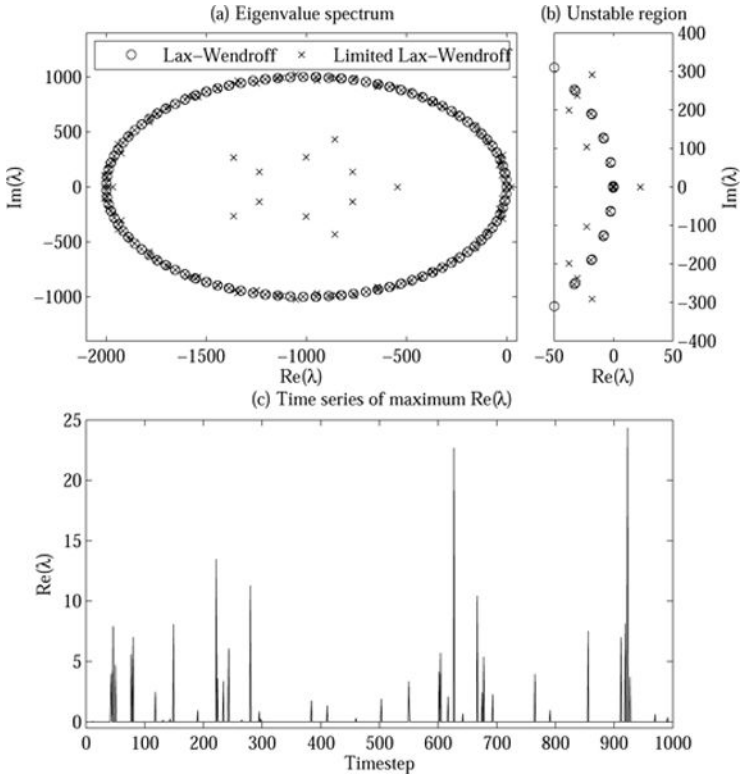

Figure 5.

As for Figure 4 but for the slotted cylinder test case with step perturbation. The spectrum in panels (a) and (b) are for time step 746.

Table 1

The normalized ℓ_2/ℓ_∞ linearity error norms, the correlation (comparing $q_N - q_N^r$ with q_L'), and the normalized ℓ_2/ℓ_∞ TLM error norms (comparing q_L' with q_T') for the Gaussian reference tracer and the Gaussian perturbation, for the 180 × 90 resolution grid. MP denotes zero to machine precision.

Gaussian Reference, Gaussian Pert	ℓ_2 linearity	ℓ_∞ linearity	Correlation	ℓ_2 TLM	ℓ_∞ TLM
Lax-Wendroff	MP	MP	1.0	0.709	0.653
Lax-Wendroff Limiter	7.42×10^{-3}	0.018	1.0	0.550	0.641
UTOPIA	MP	MP	1.0	0.377	0.442
UTOPIA Limiter	3.45×10^{-3}	0.055	1.0	0.379	0.464

Table 2

The normalized ℓ_2/ℓ_∞ linearity error norms, the correlation (comparing $q_N - q_N^r$ with q_L'), and the normalized ℓ_2/ℓ_∞ TLM error norms (comparing q_L' with q_T') for the Gaussian reference tracer and the step perturbation, for the 180 × 90 resolution grid. MP denotes zero to machine precision.

Gaussian Reference, Gaussian Pert	ℓ_2 linearity	ℓ_∞ linearity	Correlation	ℓ_2 TLM	ℓ_∞ TLM
Lax-Wendroff	MP	MP	1.0	0.918	0.891
Lax-Wendroff Limiter	0.027	0.048	1.0	0.809	0.937
UTOPIA	MP	MP	1.0	0.665	0.793
UTOPIA Limiter	0.012	0.168	1.0	0.668	0.790

Table 3

The normalized ℓ_2/ℓ_∞ linearity error norms, the correlation (comparing $q_N - q_N^r$ with q_L'), and the normalized ℓ_2/ℓ_∞ TLM error norms (comparing q_L' with q_T') for the slotted cylinder reference tracer and the Gaussian perturbation, for the 180 × 90 resolution grid. MP denotes zero to machine precision.

Slotted Cylinder Reference, Gaussian Pert	ℓ_2 linearity	ℓ_∞ linearity	Correlation	ℓ_2 TLM	ℓ_∞ TLM
Lax-Wendroff	MP	MP	1.0	0.709	0.653
Lax-Wendroff Limiter	0.119	0.273	0.993	0.589	0.648
UTOPIA	MP	MP	1.0	0.377	0.442
UTOPIA Limiter	0.285	0.445	0.960	0.434	0.461

Table 4

The normalized ℓ_2/ℓ_∞ linearity error norms, the correlation (comparing $q_N - q_N^r$ with q_L'), and the normalized ℓ_2/ℓ_∞ TLM error norms (comparing q_L' with q_T') for the slotted cylinder reference tracer and the step perturbation, for the 180 × 90 resolution grid. MP denotes zero to machine precision.

Slotted Cylinder Reference, Step Pert	ℓ_2 linearity	ℓ_∞ linearity	Correlation	ℓ_2 TLM	ℓ_∞ TLM
Lax-Wendroff	MP	MP	1.0	0.918	0.891
Lax-Wendroff Limiter	0.143	0.345	0.990	0.830	0.883
UTOPIA	MP	MP	1.0	0.665	0.793
UTOPIA Limiter	0.453	0.664	0.895	0.706	1.026

Table 5

The normalized ℓ_2 linearity error norms and the correlation (comparing $q_N - q_N^r$ with q_L') for the Gaussian reference and slotted cylinder reference tracer using the Gaussian perturbation for the 360 × 180 resolution grid.

	Gaussian Reference		Slotted Cylinder Reference	
Gaussian Perturbation	**ℓ_2 linearity**	**Correlation**	**ℓ_2 linearity**	**Correlation**
Lax-Wendroff	MP	1.0	MP	1.0
Lax-Wendroff Limiter	0.569	0.880	1.136	−0.05
UTOPIA	MP	1.0	MP	1.0
UTOPIA Limiter	4.74×10^{-4}	1.0	1.0	0.038

Table 6

The normalized ℓ_2 TLM error norms (comparing q'_L with q'_T) for the slotted cylinder reference tracer with the Gaussian perturbation for the grids composed of 180 × 90 and 360 × 180 grid points.

Slotted Cylinder Reference Gaussian Perturbation	ℓ_2 TLM 180 × 90	360 × 180
Lax-Wendroff	0.709	0.476
Lax-Wendroff Limiter	0.589	2.41
UTOPIA	0.377	0.173
UTOPIA Limiter	0.434	284.9

Table 7

The normalized ℓ_2 linearity errors, the correlation, and the ℓ_2 TLM errors for the mixed schemes for the slotted cylinder reference tracer with the Gaussian perturbation for the 180 × 90 grid point grid.

Scheme	ℓ_2 linearity	Correlation	ℓ_2 TLM
Lax-Wendroff Mix	0.415	0.879	0.709
UTOPIA Mix	0.142	0.990	0.377

Table 8

The normalized ℓ_2 linearity errors, the correlation, and the ℓ_2 TLM errors for the mixed schemes for the slotted cylinder reference tracer with the Gaussian perturbation for the 360 × 180 grid point grid.

Scheme	ℓ_2 correlation	Correlation	ℓ_2 TLM
Lax-Wendroff Mix	1.104	0.569	0.476
UTOPIA Mix	0.282	0.962	0.173